Scripta Materialia 160 (2019) 70–74

Contents lists available at ScienceDirect

Scripta Materialia

journal homepage: www.elsevier.com/locate/scriptamat

Effective evaluation of interfacial energy by matching precipitate sizes measured along a composition gradient with Kampmann-Wagner numerical (KWN) modeling

Qiaofu Zhang [a], Surendra K. Makineni [b,c], John E. Allison [b], Ji-Cheng Zhao [a,*]

[a] Department of Materials Science and Engineering, The Ohio State University, Columbus, OH 43210, USA
[b] Department of Materials Science and Engineering, University of Michigan, Ann Arbor, MI 48109, USA
[c] Department of Microstructure Physics and Alloy Design, Max-Planck-Institut für Eisenforschung GmbH, Düsseldorf 40237, Germany

ARTICLE INFO

Article history:
Received 30 September 2018
Accepted 30 September 2018
Available online xxxx

Keywords:
Interfacial energy
Phase precipitation
Nucleation and growth
KWN model
Diffusion multiples

ABSTRACT

A dual-anneal diffusion multiple was utilized to generate a composition gradient via a first anneal at a high temperature followed by a second anneal at a lower temperature to induce phase precipitation as a function of composition/supersaturation. By adjusting the interfacial energy value in simulations using the classical nucleation and growth theories as implemented in the Kampmann-Wagner numerical (KWN) model and matching the simulated average precipitate sizes at different compositions with the experimental measurements along the composition gradient, the Ni_3Al/fcc interfacial energy in the Ni-Al system at 700 °C was effectively determined to be ~12 mJ/m^2.

Precipitation is one of the most effective means to achieve high strength of materials [1–5]. Interfacial energy, γ, plays an essential role on the kinetics of precipitation and thus it is indispensable in understanding, modeling and tailoring the precipitation process to optimize materials properties. The interfacial energy is mostly measured by applying the Lifshitz-Slyozov-Wagner (LSW) theory [6,7] on the coarsening kinetics of precipitates in samples that are annealed at different time durations [8–12] or from 3D atom probe analysis of the interface chemistry [13,14].

Miyazaki [15–17] developed a method to extract interfacial energy values by: (1) making a diffusion couple and annealing it at a high temperature to create a composition gradient of a solid solution, (2) quenching the diffusion couple to ambient temperature and slicing it into several pieces parallel to the diffusion directions, (3) performing annealing of the slices of the diffusion couple at a precipitation (lower) temperature for different time durations, (4) measuring the precipitate size at the precipitation front of the samples as a function of precipitation annealing time and location (thus different supersaturation) using transmission electron microscopy (TEM), and (5) evaluating the interfacial energy value using an equation that accounts for the Gibbs-Thomson effect [18,19] with the assumption that the precipitation-front particles are at the size of the critical nucleus. This approach is still very time-consuming and labor-intensive, involving a dozen or so samples annealed at different time durations and a significant amount of TEM characterization.

The idea to be pursued under the current study is to take advantage of the particle size distribution at different locations/compositions within the composition gradient created in a dual-anneal diffusion multiple (DADM) in order to evaluate the interfacial energy by performing only *one* precipitation annealing at *one* time duration (in contrast, Miyazaki used only the precipitate size information at the precipitation-front, thus required a dozen or so different precipitation annealing experiments). Our new method requires simulations based on the classical nucleation, growth and coarsening theories as implemented via the Kampmann-Wagner numerical (KWN) model [20,21]. Our approach is to adjust the interfacial energy value in the simulations to match the simulated mean precipitate sizes at different compositions with the experimental measurements along the composition gradient such that the interfacial energy between the matrix phase and the precipitate phase can be effectively evaluated. A MatLab program implementing the KWN model was coded to facilitate the simulations, as described in the Supplementary Information. Commercially available software TC-PRISMA is also employed for the simulations and to validate the results of our KWN code.

Diffusion multiples are high-throughput samples that integrate several diffusion couples and diffusion triples into each sample [22,23]. In this way, several precipitation systems can be investigated at the same time. DADMs have been developed to effective study phase diagrams and phase precipitations by taking advantage

* Corresponding author.
E-mail address: zhao.199@osu.edu (J.-C. Zhao).

https://doi.org/10.1016/j.scriptamat.2018.09.048
1359-6462/

of the composition gradients created in DADMs [24,25]. The new approach expands the use of DADMs to enable effective evaluation of interfacial energy by integrating experimental measurements with modeling results.

The geometry of the diffusion multiples is schematically shown in Fig. 1(a) with the cross-sectional dimensions of the pieces marked; and the length perpendicular to the cross-section direction of all the pieces in Fig. 1(a) is 14 mm. Details on how to design and make

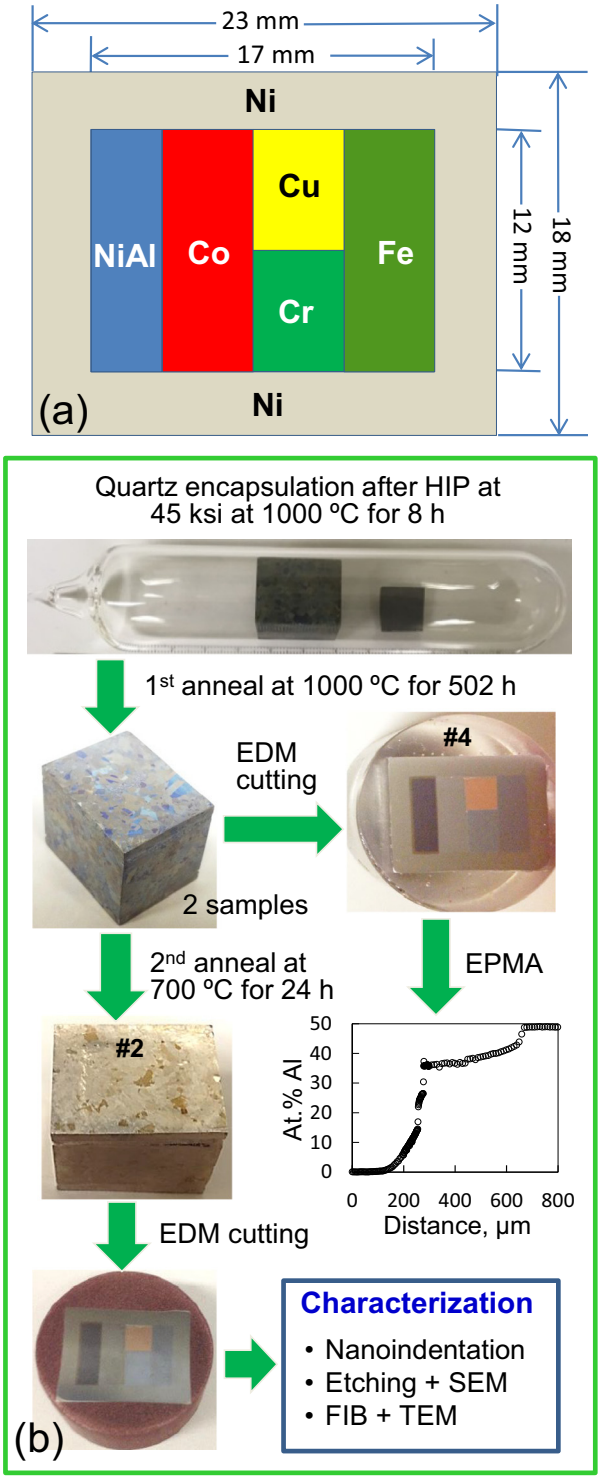

Fig. 1. Schematic cross-sectional dimensions (a) and the fabrication and analysis steps (b) of the Co-Cr-Cu-Fe-NiAl diffusion multiples.

Table 1
HIP and annealing conditions for the diffusion multiples.

Sample	HIP	First anneal	Second anneal
#1, #3, #4, #5	1000 °C, 8 h, 45 ksi	1000 °C, 502 h	
#2	1000 °C, 8 h, 45 ksi	1000 °C, 502 h	700 °C 24 h

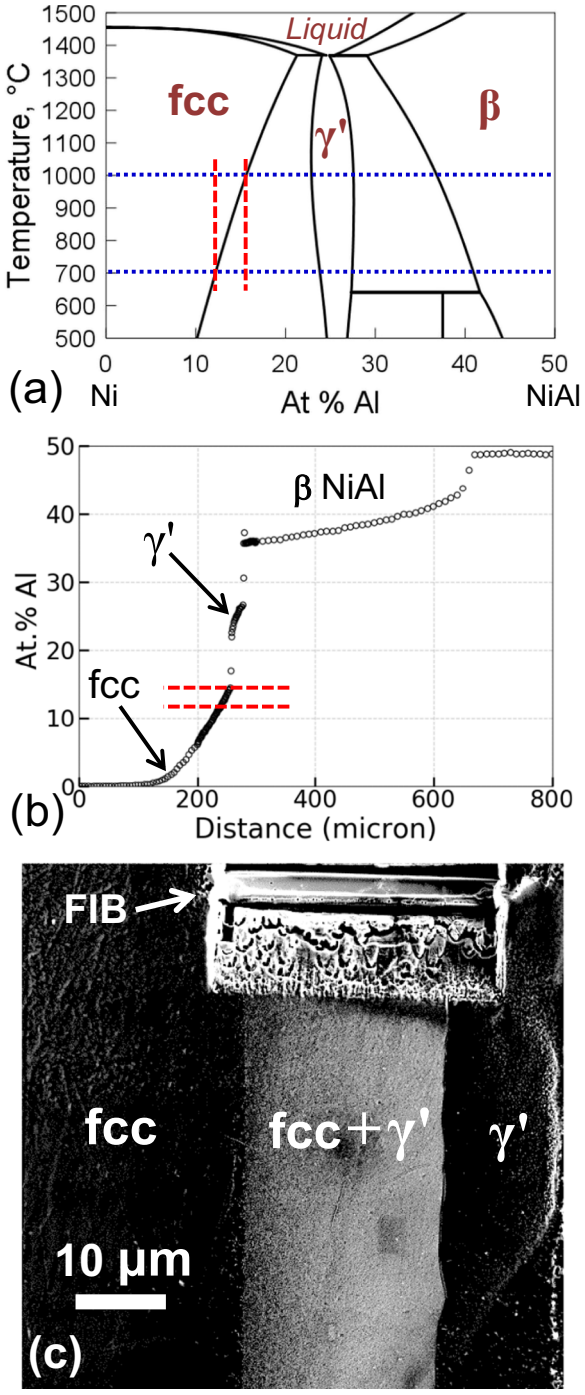

Fig. 2. The γ′ phase precipitation from the Ni-Al region of the dual anneal diffusion multiple: (a) Ni-rich part of the Ni-Al phase diagram calculated using Thermo-Calc showing the solubility difference; (b) EPMA composition profile after the first/diffusion anneal at 1000 °C 510 h; and (c) SEM image after the second/precipitation anneal at 700 °C for 24 h. The red dashed lines in (a) and (b) indicate the supersaturated area during the second anneal, which corresponds to the fcc + γ′ area in the SEM image in (c). (For interpretation of the references to color in this figure legend, the reader is referred to the web version of this article.)

successful diffusion multiples have been provided before by Zhao [26]. This geometry was designed to study phase precipitation in Ni-Al, Co-Cr, Co-Cu, Cr-Ni, Fe-Cr, and Fe-Cu binary systems. It is noted that only the Ni_3Al (γ') precipitation from the fcc Ni-Al solid solution has been studied to demonstrate the new methodology to effectively measure interfacial energy. The Ni-Al binary system was selected since the interfacial energy between the γ' precipitates and the fcc matrix phase in Ni-Al has been measured in the literature for a direct comparison. Other systems will be studied and reported in the future.

The steps for diffusion multiple preparation and analysis are shown in Fig. 1(b) and Table 1. All diffusion multiples went through a hot-isostatic pressing (HIP) process at 45 ksi (310 MPa) for 8 h to achieve intimate contacts between/among the metal pieces to allow interdiffusion to take place. The diffusion multiples were encapsulated in quartz tubes and first annealed at 1000 °C for 502 h with total time duration of 510 h (HIP and annealing) to create composition gradients via diffusion inside the samples. After the first anneal, the diffusion multiples were subjected to an immediate water quench by breaking the quartz tube to avoid the phase precipitation during cooling.

Five identical diffusion multiples were made and they all underwent the first anneal. One of the diffusion multiples (#4) were sectioned using electrical discharge machining (EDM), mounted, ground and polished for electron probe microanalysis (EPMA) to determine the compositions across the diffusion zone. The diffusion region is ~530 μm for the Ni-NiAl diffusion couple inside diffusion multiple #4 after being annealed at 1000 °C for 510 h as shown by the EPMA composition profile in Fig. 2(b). Three phases, Ni-based fcc, γ' (Ni_3Al) and B2 (β) NiAl, were observed in the diffusion region as shown in Fig. 2(b). The solubility limit for each phase from the EPMA data agrees well with the Ni-Al phase diagram showing in Fig. 2(a) that was computed using Thermo-Calc and the TCNi8 database, indicating the Gibbs free energy functions for the Ni-Al binary system is reliable.

All the other annealed diffusion multiples were encapsulated in quartz tube individually. In the present study, only one of them (#2) has been dual-annealed at 700 °C for 24 h while the other diffusion multiples will be dual-annealed at different temperatures and durations for future more systematic follow-up investigations. At the second annealing temperature of 700 °C, the compositions between the two dashed lines in Fig. 2(a) and (b) became supersaturated in Al and the γ' phase precipitated from the fcc matrix, which can be clearly seen in the SEM image in Fig. 2(c) that was taken after the diffusion multiple sample #2 was etched.

The diffusion at 700 °C for 24 h has a negligible effect on the overall composition gradient created by the first anneal at 1000 °C. A quick estimate can be made using the diffusion coefficient of Al in Ni at 700 °C ($D = 1.1 \times 10^{-18}$ m^2/s) [27]; and it yielded a diffusion distance $\sqrt{Dt} = 0.31$ μm which is negligible in comparison with the total width of ~170 μm for the fcc phase with a shallow composition gradient (~0.15 at.% Al per μm). Thus, the change in composition gradient during the second/precipitation at 700 °C can be ignored. The free energy change induced by the shallow composition gradient is also very small compared to the chemical driving force for precipitation as concluded by Miyazaki and Kobayashi via a careful analysis [28]. Therefore, each location/composition inside the composition gradient in the fcc phase, including the supersaturated composition regions between the dashed lines in Fig. 2(a) and (b), can be considered as an independent alloy during the second/precipitation anneal at 700 °C. In other words, the precipitation process under different supersaturations can be observed in one sample with the entire region showing in Figs. 2(c) and 3.

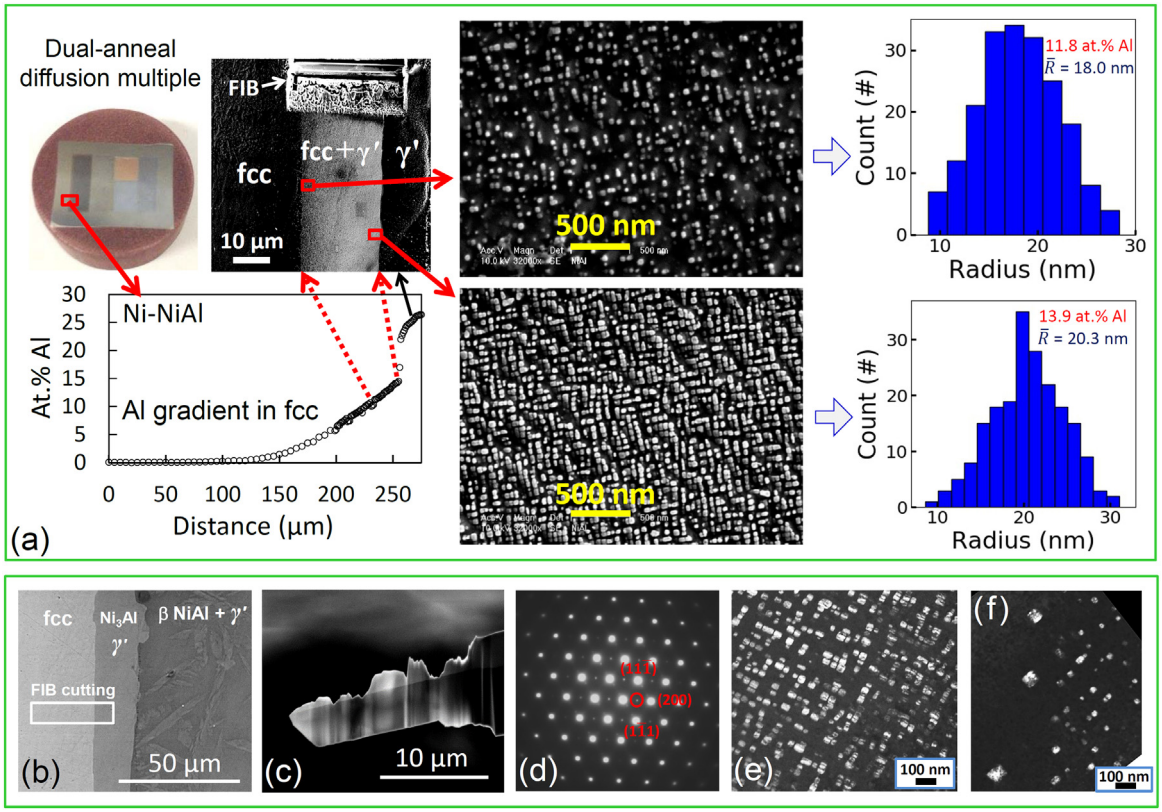

Fig. 3. Characterization the γ' precipitate sizes as a function of composition across an Al composition gradient of the fcc phase in a dual-anneal diffusion multiple: (a) HR-SEM characterization with the middle column shows HR-SEM images of the γ' precipitates at two locations/supersaturations; and (b) to (f): FIB and TEM characterization with the FIB location in (b), the TEM thin foil extracted using FIB in (c), a diffraction pattern with the ordered superlattice reflection (circled) selected for the dark-field imaging in (d), a TEM dark field image of the γ' precipitates at a location corresponding to ~11.9 at.% Al and ~17.1 μm away from the original fcc/γ' interface in (e), and a TEM dark field image showing the large γ' precipitates at the precipitate front at ~11.2 at.% Al in (f).

Since the γ′ precipitates are nm in sizes, either high resolution SEM (HR-SEM) or TEM was required to characterize their size and distribution as a function of location/composition/supersaturation. The γ′ precipitates were hard to observe even in HR-SEM without etching; and a successful etchant was developed: 30 ml lactic acid, 30 ml nitric acid, and 2 ml hydrofluoric acid. This recipe was slightly adjusted from a literature formula used for Ni-based superalloys [29]. It slightly dissolved the γ matrix in the Ni-Al system without attacking the γ′ precipitates, as clearly demonstrated in Fig. 3(a).

A number of HR-SEM images were collected along the composition gradient across the precipitation region; and particle size distribution and the mean γ′ radius were measured for each SEM image using Mipar [30] as described in more detail in the Supplementary Information.

In addition to the HR-SEM characterization, TEM was applied to characterize the γ′ precipitates on a thin foil extracted from the γ′ precipitation region using focused ion beam (FIB). The location of FIB TEM foil is visible on the top area of Fig. 2(c) and is schematically shown in Fig. 3(b). The γ′ precipitation (in the fcc matrix) region is ~21 μm adjacent to the original fcc/γ′ phase interface; and the FIB foil was extended to 25 μm to make sure the entire γ′ precipitation region was covered in the TEM foil. The TEM foil was tilt to the [0$\bar{1}\bar{1}$] direction such that the reflections from both the fcc matrix and γ′ precipitates can be clearly seen and a superlattice reflection from the γ′ phase was selected to collect a TEM dark field image of the γ′ precipitates, Fig. 3(e). Similarly, the entire TEM foil, which had the composition gradient, was scanned and a number of TEM dark field images were taken (Several of them are shown in the Supplementary Information). The γ′ precipitate sizes and distributions were measured from the TEM dark field images again using Mipar.

All the experimental data for the mean γ′ precipitate radius obtained from both HR-SEM and TEM images are summarized and plotted in Fig. 4(a) as a function of supersaturation. The change of the γ′ precipitate radius with decreasing supersaturation is relatively small until reaching the reaction front, where the γ′ precipitates became much larger, which can be clearly seen in Fig. 3(f) as well – similar to the observations of Miyazaki. More detailed results with standard deviations are shown in Fig. 4(b). With decreasing supersaturation, the particle number density decreases until it reaches a minimum at the precipitate front as described in the Supplementary Information.

On the modeling side, a MatLab based program was developed to simulate the precipitation process based on the classic nucleation, growth, and coarsening theories as implemented in the KWN model [20,21]. Several elegant reviews on the KWN simulations are available in the literature [21,31–33]. Our simulation process follows these implementations as described in the Supplementary Information. For simplicity, only homogenous precipitation is described in this study and the matrix is treated as homogenous under the mean field assumption. The purpose of developing our own KWN code is to allow more flexibility to investigate the precipitation evolution by varying parameters in simulations that may not be available in commercial codes.

Both our KWN program code and the commercial KWN software TC-PRISMA were applied to simulate the γ′ precipitate radius and particle density using the same thermodynamic database (TCNi8) and the same parameters listed in Table 2. The interfacial energy γ was set as an adjustable input parameter ranging from 10 to 20 mJ/m^2. For each interfacial energy value, several compositions (supersaturations) were simulated and the results are plotted as lines in Fig. 4(a) and (b) (Only the results of 10, 12 and 14 mJ/m^2 are plotted for simplicity). Good agreement between the results from our KWN program code and TC-PRISMA suggests the reliability of our own code. The slight difference between the simulated results is due to small differences in numerical settings.

It is concluded from Fig. 4 that the measured interfacial energy between the fcc matrix phase and the γ′ precipitates in the Ni-Al binary system at 700 °C is ~12 mJ/m^2. This value is very close to the value of 14 mJ/m^2 reported by Miyazaki as shown in Fig. 4(c) which compares our measured interfacial energy value with most literature values

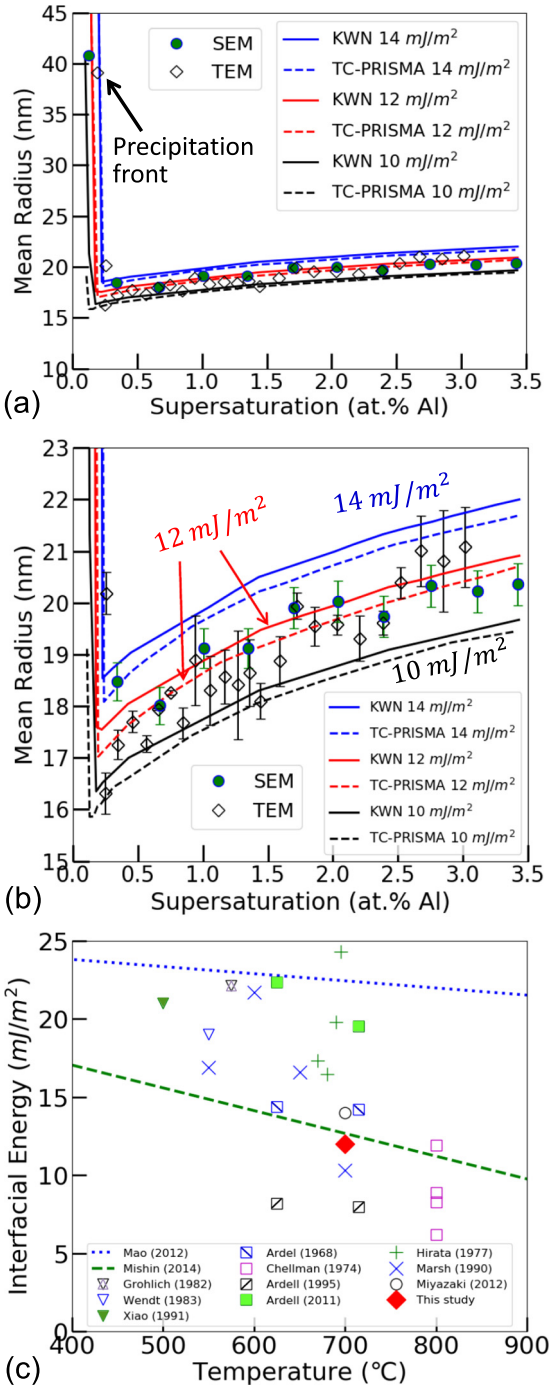

Fig. 4. Comparison between the simulated (lines) and experimentally measured (symbols) γ′ mean precipitate radius as a function of Al supersaturation: (a) overall comparison including the precipitate radius at the precipitate front; and (b) detailed comparison without the γ′ precipitate front data. The simulation results via our own KWN modeling code using 3 interfacial energy values (10, 12 and 14 mJ/m^2) are plotted as solid lines and those from TC-PRISMA are shown as dashed lines. (c) Comparison of our γ′/fcc interfacial energy value for the Ni-Al binary system with most other experimental measurements (symbols) [8,9,12,15,34–39] and computed results (lines) [40–46] reported in the literature (Only two representative computational results (lines) are plotted in (c) for simplicity).

from both experimental measurements (showing as symbols in Fig. 4(c)) [8,9,12,15,34–39] and computer simulations (showing as lines in Fig. 4(c)) [40–46] including Monte Carlo simulations with an embedded-atom potential via a so-called capillary fluctuation method [41]. The experimental values reported in the literature vary from ~6

Table 2
Conditions for the γ′ precipitation simulations.

Thermodynamic database	Diffusion coefficient (m^2/s)	Precipitation anneal time (h)	Precipitation temperature (°C)	Equilibrium composition of γ′, X^P (at.% Al)	Equilibrium composition of fcc, X^e (at.% Al)
TCNi8	1.1×10^{-18}	24	700	23.1	11.57

to ~26 mJ/m^2 at temperatures close to our measurement (700 °C) and our data is in the middle of these values. Interestingly, our data is in excellent agreement with the computed values from Mishin using the capillary fluctuation method as shown in Fig. 4(c).

The reliability of our interfacial energy value is supported by the good agreement between the experimental results and independent TC-PRISMA simulations using an interfacial energy value of 12 mJ/m^2, as shown in Fig. 4(b). In the absence of more experimental data, it is recommended that the temperature-dependent interfacial energy fitted from Mishin's computed data be used for the γ′ precipitation simulations for the Ni-Al alloys (until/unless future experimental results prove otherwise). The recommended γ′/fcc interfacial energy is $\gamma = 26.4 - 0.0142 \times T$ mJ/m^2 (T in Kelvin).

It would be very prudent to explore whether the excellent agreement between our measured interfacial energy value and Mishin's calculations is a fortunate coincidence or the capillary fluctuation method has good reliability in computing the interfacial energy. This can be accomplished by performing experimental measurements and computer simulations of a few precipitation systems of interest in the future. Confirmation of the reliability of a computational approach would help provide a large amount of reliable computed data since experimental measurements can only be performed on a limited number of systems even with a high-throughput approach as described in this study.

In summary, a set of Co-Cr-Cu-Fe-NiAl diffusion multiples were made and first annealed at 1000 °C for 510 h to create composition gradients in the diffusion couples inside these diffusion multiples. One of these diffusion multiples was dual-annealed at 700 °C for 24 h to induce phase precipitation in the supersaturated compositions along the composition gradients. HR-SEM and TEM were employed to evaluate the γ′ precipitate size and distribution in the Ni-NiAl diffusion couple region of the dual-anneal diffusion multiple. A MatLab code was created to simulate the homogenous phase precipitation process using the KWN model and to adjust the interfacial energy value to match the experimental results at different compositions. The best match yielded an interfacial energy value of ~12 mJ/m^2 for the γ′ precipitation from the fcc Ni-Al solid solution at 700 °C, which is within the ~6 to ~25 mJ/m^2 value range reported by various research groups. The good agreement between the experimental and simulation results using an independent program – TC-PRISMA – lends confidence on our interfacial energy value as well as our own KWN code.

Acknowledgement

This work was mainly supported by the U.S. National Science Foundation (NSF) under grant number 1237577 at The Ohio State University. The TEM work was supported by the Ford Motor Company. Our own KWN modeling code written in MatLab is available upon request from the authors.

Appendix A. Supplementary data

Supplementary data to this article can be found online at https://doi.org/10.1016/j.scriptamat.2018.09.048.

References

[1] J.W. Martin, Precipitation Hardening: Theory and Applications, 2nd ed. Butterworth-Heinemann, 1998.
[2] A.J. Ardell, Metall. Trans. A. 16 (1985) 2131–2165.
[3] R.E. Smallman, A.H.W. Ngan, Mod. Phys. Metall. Elsevier, 2014 499–527.
[4] A. Argon, Strengthening Mechanisms in Crystal Plasticity, Oxford University Press, 2007.
[5] T. Gladman, Mater. Sci. Technol. 15 (1999) 30–36.
[6] I.M. Lifshitz, V.V. Slyozov, J. Phys. Chem. Solids 19 (1961) 35–50.
[7] C. Wagner, Z. Elektrochem. 65 (1961) 581–591.
[8] A. Ardell, Interface Sci. 3 (1995) 119–125.
[9] A.J. Ardell, J. Mater. Sci. 46 (2011) 4832–4849.
[10] P.W. Voorhees, J. Stat. Phys. 38 (1985) 231–252.
[11] A.J. Ardell, R.B. Nicholson, J. Phys. Chem. Solids 27 (1966) 1793–1794.
[12] A.J. Ardell, Acta Metall. 16 (1968) 511–516.
[13] C.K. Sudbrack, K.E. Yoon, R.D. Noebe, D.N. Seidman, Acta Mater. 54 (2006) 3199–3210.
[14] E.Y. Plotnikov, Z. Mao, R.D. Noebe, D.N. Seidman, Scr. Mater. 70 (2014) 51–54.
[15] T. Miyazaki, Prog. Mater. Sci. 57 (2012) 1010–1060.
[16] T. Miyazaki, T. Koyama, S. Kobayashi, Metall. Mater. Trans. A 30 (1999) 2783–2789.
[17] T. Miyazaki, T. Koyama, S. Kobayashi, Metall. Mater. Trans. A 27 (1996) 945–949.
[18] M. Perez, Scr. Mater. 52 (2005) 709–712.
[19] Q. Du, M. Perez, W.J. Poole, M. Wells, Scr. Mater. 66 (2012) 419–422.
[20] R. Kampmann, R. Wagner, Decompos. Alloy. Early Stages, Elsevier, 1984 91–103.
[21] R. Wagner, R. Kampmann, P.W. Voorhees, Mater. Sci. Technol. Wiley-VCH Verlag GmbH & Co. KGaA, Weinheim, Germany, 2013 309–407.
[22] J.-C. Zhao, Adv. Eng. Mater. 3 (2001) 143–147.
[23] J.-C. Zhao, Prog. Mater. Sci. 51 (2006) 557–631.
[24] S. Cao, J.-C. Zhao, Acta Mater. 88 (2015) 196–206.
[25] S. Cao, J.-C. Zhao, J. Phase Equilib. Diffus. 37 (2016) 25–38.
[26] J.-C. Zhao, Methods Phase Diagr. Determ. Elsevier, 2007 246–272.
[27] W. Gust, M.B. Hintz, A. Loddwg, H. Odelius, B. Predel, Phys. Status Solidi 64 (1981) 187–194.
[28] T. Miyazaki, S. Kobayashi, Philos. Mag. 90 (2010) 305–316.
[29] T.M. Smith, B.D. Esser, N. Antolin, G.B. Viswanathan, T. Hanlon, A. Wessman, D. Mourer, W. Windl, D.W. McComb, M.J. Mills, Acta Mater. 100 (2015) 19–31.
[30] J.M. Sosa, D.E. Huber, B. Welk, H.L. Fraser, Integr. Mater. Manuf. Innov. 3 (2014) 10.
[31] M. Perez, M. Dumont, D. Acevedo-Reyes, Acta Mater. 56 (2008) 2119–2132.
[32] O.R. Myhr, Ø. Grong, Acta Mater. 48 (2000) 1605–1615.
[33] J.D. Robson, P.B. Prangnell, Acta Mater. 49 (2001) 599–613.
[34] H. Wendt, P. Haasen, Acta Metall. 31 (1983) 1649–1659.
[35] S.Q. Xiao, P. Haasen, Acta Metall. Mater. 39 (1991) 651–659.
[36] D. Chellman, A. Ardell, Acta Metall. 22 (1974) 577–588.
[37] C. Marsh, H. Chen, Acta Metall. Mater. 38 (1990) 2287–2298.
[38] M. Gröhlich, P. Haasen, G. Frommeyer, Scr. Metall. 16 (1982) 367–370.
[39] T. Hirata, D.H. Kirkwood, Acta Metall. 25 (1977) 1425–1434.
[40] Z. Mao, C. Booth-Morrison, E. Plotnikov, D.N. Seidman, J. Mater. Sci. 47 (2012) 7653–7659.
[41] Y. Mishin, Model. Simul. Mater. Sci. Eng. 22 (2014) 045001.
[42] X.L. Liu, S.-L. Shang, Y.-J. Hu, Y. Wang, Y. Du, Z.-K. Liu, Mater. Des. 133 (2017) 39–46.
[43] D. Farkas, M.F. de Campos, R.M. de Souza, H. Goldenstein, Scr. Metall. Mater. 30 (1994) 367–371.
[44] D.L. Price, B.R. Cooper, MRS Proc. 408 (1995) 463–468.
[45] A.J. Ardell, V. Ozolins, Nat. Mater. 4 (2005) 309–316.
[46] C. Woodward, A. van de Walle, M. Asta, D.R. Trinkle, Acta Mater. 75 (2014) 60–70.